Validation of a DNS code for wall-bounded turbulence including finite-rate reactions and surface catalysis

L. Duan and M. Pino Martín

Mechanical and Aerospace Engineering
Princeton University, Princeton NJ 08544

Abstract

This paper discusses the constitutive relations, surface catalytic model, and numerical methods for direct numerical simulation (DNS) of wall-bounded turbulence including finite-rate chemistry and gas-surface interaction. The validation of the code is provided for the mean flow by comparison to similarity solutions and laminar hypersonic boundary layer solutions, for the surface catalysis by comparison to analytic solutions for the one-dimensional diffusion-reaction equation, and for turbulent boundary layers by comparison to empirical predictions.

1 Introduction

The boundary layers that are formed on hypersonic vehicles are hot, chemically reacting, and turbulent. Currently, the boundary layer on realistic hypersonic vehicles is simulated either assuming that the boundary layer is laminar or using simple models that have not been calibrated for hypersonic applications. Generally, the calibration of turbulent models has been done using DNS databases of incompressible flows or using perfect gas wind tunnel data. As a result, the chemical composition of gas, the skin friction, and the heat transfer are not predicted accurately. If we were able to perform more accurate simulations of hypersonic flows, we may find a different chemical composition of the gas, and different heating rates than those that are currently predicted.

In our previous work [1, 2, 3], we used DNS to perform fundamental studies of hypersonic turbulent boundary layers. We found that small magnitude of the temperature fluctuations results in large variations in the reaction rates. In addition, the turbulent motion is enhanced by the exothermic reactions, while is damped by endothermic reactions. This is a feedback process that takes place through the pressure-strain term in the Reynolds stress equation. Furthermore, the magnitude of temperature fluctuations scales with mean flow

variables. These results have also been observed in DNS of reacting isotropic turbulence [4, 5].

Various assumptions are made in our previous work. First, the vibrational mode of gas species is neglected and the heat capacity of each species is held constant. Second, a power law is applied to calculate mixture's viscosity. However, the power law is only valid in a narrow range of temperatures (about 100 K to 2000 K) relative to the temperatures that can be found in hypersonic boundary layers. Third, the effect of wall catalysis is neglected. Although some of these assumptions make the analysis relatively simpler to extract the physics of the problem, it is also necessary to generalize the analysis to include vibrational process and surface catalysis.

This paper provides a description of the constitutive relations, numerical methods, and validation of our original DNS code for wall-bounded turbulence, which has been generalized to include real gas effects and wall catalysis. The validation includes both mean flow field and turbulence. The mean flow field is validated against a similarity solution, solutions provided by DPLR [6], which is a parallel multiblock finite-volume code that solves the Navier-Stokes equations including finite-rate chemistry and the effects of thermal nonequilibrium, and recently published data of diffusion tube experiments including wall catalysis [7]. The turbulence field is validated against theoretical results and experimental data.

2 Governing equations and constitutive relations

The equations describing the unsteady motion of a reacting fluid are given by the species mass, mass-averaged momentum, and total energy conservation equations, which, neglecting thermal nonequilibrium, are

$$\begin{aligned}
\frac{\partial \rho_s}{\partial t} + \frac{\partial}{\partial x_j}\Big(\rho_s u_j + \rho_s v_{sj}\Big) &= w_s \\
\frac{\partial \rho u_i}{\partial t} + \frac{\partial}{\partial x_j}\Big(\rho u_i u_j + p\delta_{ij} - \sigma_{ij}\Big) &= 0 \\
\frac{\partial E}{\partial t} + \frac{\partial}{\partial x_j}\Big((E+p)u_j - u_i\sigma_{ij} + q_j + \sum_s \rho_s v_{sj} h_s\Big) &= 0
\end{aligned} \tag{1}$$

where w_s represents the rate of production of species s due to chemical reactions; ρ_s is the density of species s; u_j is the mass-averaged velocity in the j direction; v_{sj} is the diffusion velocity of species s described in Section 2.1; p is the pressure, which is given by

$$p = \sum_s \rho_s \frac{\hat{R}}{M_s} T \ , \tag{2}$$

where $\hat{R}$ is the universal gas constant, M_s is the molecular weight of species s, and T is the translational temperature; σ_{ij} is the shear stress tensor, which is

given by a linear stress-strain relationship

$$\sigma_{ij} = 2\mu S_{ij} - \frac{2}{3}\mu\delta_{ij}S_{kk}, \tag{3}$$

where $S_{ij} = \frac{1}{2}(\partial u_i/\partial x_j + \partial u_j/\partial x_i)$ is the strain rate tensor, μ is the mixture viscosity discussed in Section 2.2; h_s is the specific enthalpy of species s; q_j is the heat flux due to temperature gradients, which is given by Fourier's law

$$q_j = -\kappa\frac{\partial T}{\partial x_j}\ , \tag{4}$$

where κ is the mixture thermal conductivity described in Section 2.2; and E is the total energy per unit volume given by

$$E = \sum_s \rho_s c_{vs} T + \sum_s E_{vs} + \frac{1}{2}\rho u_i u_i + \sum_s \rho_s h_s^\circ, \tag{5}$$

where c_{vs} is the translational-rotational specific heat at constant volume of species s, given by

$$c_{vs} = c_{vtr\ s} + c_{vrot\ s} \tag{6}$$

with the translational and rotational specific heats are given by

$$c_{vtr\ s} = \frac{3}{2}\frac{\hat{R}}{M_s} \qquad c_{vrot\ s} = \frac{\hat{R}}{M_s}\ , \tag{7}$$

and $cv_{rot\ s}$ is zero for monatomic species; and h° is the heat of formation of species. E_{vs} is the vibrational energy of species s, given by

$$E_{vs} = \rho_s\frac{\hat{R}}{M_s}\frac{\theta_{vs}}{\exp(\theta_{vs}/T) - 1}\ , \tag{8}$$

where θ_{vs} is the characteristic temperature of vibration for species s. The diffusion model, the calculation of the multicomponent mixture transport coefficients μ, κ and species diffusivity, and the chemical source terms are described in the following sections.

2.1 Diffusion model

Two diffusion models are considered: a Fickian diffusion model, which is used when considering a single binary reaction mechanism, and a more general self-consistent effective binary diffusion model [8] for a mixture of species.

2.1.1 Fick's diffusion model

In this case, the diffusion of species is given by

$$J_{sj} = \rho_s v_{sj} = -\rho D\frac{\partial c_s}{\partial x_j}, \tag{9}$$

where c_s is the mass fraction, $c_s = \rho_s/\rho$; and D is the diffusion coefficient, which is equal for all species and given in terms of the Lewis number

$$D = \frac{\kappa Le}{\rho C_p}, \tag{10}$$

where Le is the Schmidt number.

2.1.2 Multicomponent diffusion model

A more accurate representation for a multicomponent mixture is the self-consistent effective binary diffusion (SCEBD) model [8]. This method allows for the variation of species diffusion coefficients.

The effective binary diffusivities for non-electron pairings are

$$D_s = \left(1 - \frac{\chi_s}{\chi}\right)\left(\sum_{r \neq s} \frac{x_r}{D_{r,s}}\right)^{-1}, \tag{11}$$

where x_s is the mole fraction of species s; $D_{r,s}$ is the temperature dependent binary diffusion transport coefficient, which is described in the following section; and χ_s/χ is the friction coefficient, defined as

$$\frac{\chi_s}{\chi} = \frac{\rho_s/M_s}{\sum_s \rho_s/M_s}. \tag{12}$$

To assume non-ionization of all species, the mass flux is given by

$$\vec{J}_s = \rho_s \vec{v}_s = -\left(cM_s D_s\right) \nabla\left(x_s\right) + \frac{\rho_s}{\rho} \sum \left(cM_r D_r\right) \nabla\left(x_r\right) \ , \tag{13}$$

where c is the molar density of the gas.

2.2 Mixture transport properties

The transport properties required to solve Eq. 1 are the viscosity, thermal conductivity and species binary diffusion coefficients. These transport properties depend on the cross sections for collisions between species i and j. The collision integrals provide an accurate representation of the interaction between different particles, molecules and atoms, as well as ionized species. For a first-order approximation of the Chapman-Enskog theory, we only need to consider the diffusion collision integral $\Omega_{ij}^{1,1}$ and the viscosity collision integral $\Omega_{ij}^{2,2}$.

2.2.1 Collision integrals

Gupta *et al.* [9] provide curve fits for each collision integral. For collisions not involving charged particle interaction, the collision integral is given by

$$\pi\Omega_{ij}^{(l,s)}(T) = 10^{-20} D_{ij}^{(l,s)} T^{A_{ij}^{(l,s)}(lnT)^2 + B_{ij}^{(l,s)}(lnT)^2 + C_{ij}^{(l,s)}} \tag{14}$$

Where $A_{ij}^{(l,s)}$, $B_{ij}^{(l,s)}$, $C_{ij}^{(l,s)}$, $D_{ij}^{(l,s)}$ are curve fit coefficients, which can be obtained from Wright *et al.* [10].

2.2.2 Binary diffusion coefficients

The binary diffusion transport coefficients appearing in Eq. 11 are defined as

$$D_{r,s} = \frac{3}{16p\pi\Omega_{r,s}^{(1,1)}}\sqrt{\frac{2\pi\left(k_B T\right)^3}{\mathcal{M}_{r,s}}} \tag{15}$$

with

$$\mathcal{M}_{i,j} = \frac{M_i M_j}{M_i + M_j} N_A^{-1}$$

where k_B is the Boltzmann's constant 1.381×10^{-23}J/K, N_A is Avogadro's number $6.022 \times 10^{23}\text{mol}^{-1}$.

2.2.3 Multicomponent mixture viscosity

The mixture viscosity is given by a second-order multicomponent Gupta[9] method,

$$\mu = \sum_{i=1}^{ns}\left(\frac{x_i M_i/N_A}{\sum_{j=1}^{ns} x_j \Delta_{ij}^{(2)}}\right) \tag{16}$$

where n_s is the number of species and

$$\Delta_{ij}^{(2)} = \frac{16}{5} 1.0 \times 10^{-20}\left(\frac{2M_i M_j}{\pi \hat{R} T (M_i + M_j)}\right)^{1/2} \pi\Omega_{ij}^{(2,2)} \tag{17}$$

2.2.4 Multicomponent mixture thermal conductivity

The mixture frozen thermal conductivity is calculated from a modified Eucken relation,[11]

$$\kappa = \kappa_{\text{tr}} + \kappa_{\text{int}}, \tag{18}$$

where κ_{tr} and κ_{int} are the mixture translational and internal components of the thermal conductivity. These are given by a second-order multicomponent Gupta[9]-Yos[12] method.

$$\kappa_{\text{int}} = k_B \sum_{i=1}^{ns}\left[\frac{\left(\frac{c_{pi}}{\hat{R}} - \frac{5}{2}\right) x_i}{\sum_{j=1}^{ns} x_j \Delta_{ij}^{(1)}}\right] \tag{19}$$

where c_{ps} is the specific heat at constant pressure of species s; and $\Delta_{ij}^{(1)}$ is given by

$$\Delta_{ij}^{(1)} = \frac{8}{3} 1.0 \times 10^{-20}\left(\frac{2M_i M_j}{\pi \hat{R} T (M_i + M_j)}\right)^{1/2} \pi\Omega_{ij}^{(1,1)} \tag{20}$$

The translational component of the mixture thermal conductivity is given by

$$\kappa_{\text{tr}} = \frac{15}{4} k_B \sum_{i=1}^{ns}\left(\frac{x_i}{\sum_{j=1}^{ns} \alpha_{ij} x_j \Delta_{ij}^{(2)}}\right) \tag{21}$$

where

$$\alpha_{ij} = 1 + \frac{(1 - (M_i/M_j))\,(0.45 - 2.54(M_i/M_j))}{(1 + (M_i/M_j))^2} \tag{22}$$

2.3 Gas-phase reactions

We consider two reduced chemical mechanisms with increasing complexity. Namely, a simplified two-species mechanism: N_2, N with Arrhenius parameters [13]; and a five-species mechanism: N_2, O_2, NO, N, and O with Arrhenius parameters [13]. The five-species mechanism represents the realistic reactions of air before ionization happens, which is a good approximation at temperatures less than about $10,000$K. The corresponding equilibrium constants are computed from the Gibbs free energy as functions of temperature and then fitted to Park (1990) expressions [13]. For simplicity ionization and ablation effects are neglected.

2.3.1 Two species mechanism

The two-species mechanism includes N_2, N. Thus, the reaction mechanism is governed by a single dissociation reaction given as

$$N_2 + M \rightleftharpoons 2N + M \tag{23}$$

where M is a collision partner, either N_2 or N in this case. Let us label this reaction as R_1. The source terms for the species are

$$w_{N_2} = -w_N = -M_{N_2} k_f \frac{\rho_{N_2}}{M_{N_2}} \left(\frac{\rho_{N_2}}{M_{N_2}} + \frac{\rho_N}{M_N} \right) + M_{N_2} k_b \left(\frac{\rho_N}{M_N} \right)^2 \left(\frac{\rho_{N_2}}{M_{N_2}} + \frac{\rho_N}{M_N} \right) \tag{24}$$

where k_f and k_b are the forward and backward Arrhenius reaction rates, respectively.

These are written as

$$k_{fm} = C_{fm} T^{\eta_m} e^{-\theta_{dm}/T} \qquad k_b = k_f / K_{\text{eq}} \tag{25}$$

where K_{eq} is the temperature dependent equilibrium constant described by Park[13] as

$$K_{\text{eq}} = 10^{-6} \exp\left(A_1/Z + A_2 + A_3 ln(Z) + A_4 Z + A_5 Z^2 \right) \ , \tag{26}$$

where $Z = 10,000/T$ with T in Kelvin, and As are curve-fit coefficients. The Arrhenius coefficients in Eq. 25 and the curve-fit coefficients in Eq. 26 are given in Tables 1 and 2.

2.3.2 Five species mechanism

The five-species mechanism includes N_2, O_2, NO, N, and O. Thus, the reaction mechanism is governed by

$$N_2 + M \quad \rightleftharpoons \quad 2N + M$$

$$\begin{aligned} O_2 + M &\rightleftharpoons 2O + M \\ NO + M &\rightleftharpoons N + O + M \\ N_2 + O &\rightleftharpoons NO + N \\ NO + O &\rightleftharpoons O_2 + N \end{aligned} \tag{27}$$

We label the first, second, third, fourth, fifth of these reactions as R_1, R_2, R_3, R_4, R_5 respectively. Each of these reactions is governed by a forward and backward rate coefficients, k_{fm} and k_{bm}. Therefore, we write the rate of each reaction as a sum of the forward and backward rates

$$\begin{aligned} \mathcal{R}_1 &= \sum_m \left[k_{b1m} \left(\frac{\rho_N}{M_N} \right)^2 \frac{\rho_m}{M_m} - k_{f1m} \frac{\rho_{N_2}}{M_{N_2}} \frac{\rho_m}{M_m} \right] \\ \mathcal{R}_2 &= \sum_m \left[k_{b2m} \left(\frac{\rho_O}{M_O} \right)^2 \frac{\rho_m}{M_m} - k_{f2m} \frac{\rho_{O_2}}{M_{O_2}} \frac{\rho_m}{M_m} \right] \\ \mathcal{R}_3 &= \sum_m \left[k_{b3m} \frac{\rho_N}{M_N} \frac{\rho_O}{M_O} \frac{\rho_m}{M_m} - k_{f3m} \frac{\rho_{N_2}}{M_{N_2}} \frac{\rho_m}{M_m} \right] \\ \mathcal{R}_4 &= k_{b4} \frac{\rho_{NO}}{M_{NO}} \frac{\rho_N}{M_N} - k_{f4} \frac{\rho_{N_2}}{M_{N_2}} \frac{\rho_O}{M_O} \\ \mathcal{R}_5 &= k_{b5} \frac{\rho_{O_2}}{M_{O_2}} \frac{\rho_N}{M_N} - k_{f5} \frac{\rho_{NO}}{M_{NO}} \frac{\rho_O}{M_O} \end{aligned} \tag{28}$$

so that the chemical source terms can be expressed in terms of the individual reaction rates, $\mathcal{R}_s$

$$\begin{aligned} w_{N2} &= M_{N2} (\mathcal{R}_2 + \mathcal{R}_4) \\ w_{O2} &= M_{O2} (\mathcal{R}_2 - \mathcal{R}_5) \\ w_{NO} &= M_{NO} (\mathcal{R}_3 - \mathcal{R}_4 + \mathcal{R}_5) \\ w_N &= M_N (-2\mathcal{R}_1 - \mathcal{R}_3 - \mathcal{R}_4 - \mathcal{R}_5) \\ w_O &= M_O (-2\mathcal{R}_2 - \mathcal{R}_3 + \mathcal{R}_4 + \mathcal{R}_5) \end{aligned} \tag{29}$$

C_{fm}, η_m, and θ_{dm} are given in Table 1

3 Species boundary conditions

The production of species by surface-catalyzed reactions must be balanced by their diffusive flux at the wall:

$$J_{s,w} = w_{s,w} \tag{30}$$

where the subscript "w" represents wall quantities. For reactant species the production rates at the surface can be expressed as a loss probability, γ_s, times the surface impingement fluxes; for O and N this gives the production rates (negative for loss)

$$w_{O,w} = -\gamma_O \frac{\rho_{O,w} \bar{v}_O}{4}$$

$$w_{N,w} = -\gamma_N \frac{\rho_{N,w}\bar{v}_N}{4} \tag{31}$$

where $\bar{v}_s = \sqrt{\frac{8\hat{R}T}{\pi M_s}}$ is the average thermal velocity of species s.

The loss probability is defined as the fraction of impinging reactant flux removed permanently from the gas phase. It is not a fundamental chemical quantity, rather, it reflects the total efficiency of all operating surface reaction pathways that remove species s on a particular combination of temperature, pressure, and gas composition. If the reactant species is consumed to produce more than one product species, branching fractions, $f_{s,r}$, can be defined as the fraction of impinging reactant removed permanently from the gas phase that participates in forming product species r.

The absolute lower and upper bounds on both γ_s and $f_{s,r}$ are 0 and 1, but this range may be reduced by other factors such as the availability of partner reactants. For a partially dissociated gas mixture of oxygen and nitrogen interacting with a catalytic surface via three net steady-state heterogeneous reaction pathways: $O+O \rightarrow O_2$, $N+N \rightarrow N_2$, and $O+N \rightarrow NO$, element conservation dictates the constraint:

$$(1 - f_{O,O_2}) \frac{\gamma_O \rho_{O,w} \bar{v}_O}{M_O} = (1 - f_{N,N_2}) \frac{\gamma_N \rho_{N,w} \bar{v}_N}{M_N} \tag{32}$$

The individual production rates of the surface reaction products are

$$\begin{aligned} w_{O_2,w} &= -f_{O,O_2} \frac{M_{O_2}}{2M_O} w_{O,w} \\ w_{N_2,w} &= -f_{N,N_2} \frac{M_{N_2}}{2M_N} w_{N,w} \\ w_{NO,w} &= (f_{N,N_2} - 1) \frac{M_{NO}}{2M_N} w_{N,w} = (f_{O,O_2} - 1) \frac{M_{NO}}{2M_O} w_{O,w} \end{aligned} \tag{33}$$

where the loss probability and branching factor of species are obtained from experiments.

4 Numerical method

We solve the equations governing unsteady fluid motion in conservative form, namely the conservative form of the chemical species mass, momentum, and energy equations. In DNS, the equations are solved with no modeling assumption. Thus, DNS allows for the accurate and detailed simulation of fluid flows in the laminar to turbulent regimes. Turbulent flow calculations are significantly more challenging than their laminar counterparts, as all turbulent length and time scales must be resolved.

The spatial derivatives are computed using a fourth-order accurate WENO scheme.[14, 15, 16] To perform the numerical integration, we use a second-order, implicit Data-Parallel, Lower-Upper, Relaxation technique [17]. The viscous terms are computed using a fourth-order accurate central scheme. A Newton-Raphson method is used to obtain the temperature from Eq. 5.

5 Code validation

5.1 Similarity solution for laminar flow

A similarity solution can be obtained by performing a similarity transformation of the partial differential boundary layer equations to transform them to ordinary differential equations (ODE) [18, 19].

Let us introduce the following definitions:

$$\begin{aligned} \xi &= \rho_e \mu_e u_e x \\ \eta &= \frac{u_e}{\sqrt{2\xi}} \int_0^y \rho dy \\ f' &= \frac{df}{d\eta} = \frac{u}{u_e} \\ g &= \frac{h_0}{h_{e0}} \\ s_A &= \frac{cs_A}{cs_{Ae}} \end{aligned}$$

Let Pr be the Prandtl number, $Pr = \frac{c_p \mu}{\kappa}$, $C = \frac{\rho\mu}{\rho_e \mu_e}$ and Ec is the Eckert number, which is defined here as $\frac{u_e^2}{h_{0e}}$. For flow over a flat plate, assuming chemically frozen boundary layer with $Pr = \text{const}$, $Le = 1$, $C = \text{const}$, the original set of partial differential equations, namely species continuity, momentum and energy equations, respectively, can be written as:

$$\begin{gathered} \frac{d}{d\eta}\left(\frac{C}{Pr} s'_A\right) + f s'_A = 0 \\ (Cf'')' + f f'' = 0 \\ \frac{d}{d\eta}\left(\frac{C}{Pr} g'\right) + f g' + Ec \frac{d}{d\eta}\left(\left(1 - \frac{1}{Pr}\right) C f' f''\right) = 0 \end{gathered} \tag{34}$$

The above equations have been written for a binary gas. For multicomponent gases there are additional species equations. By defining

$$\begin{aligned} f_1 &= f \\ f_2 &= f' \\ f_3 &= Cf'' \\ s_1 &= s_A \\ s_2 &= s'_A \frac{C}{Pr} \\ g_1 &= g \\ g_2 &= g' \frac{C}{Pr} \end{aligned}$$

the above set of ODEs can be cast into a 1st oder system of ODEs

$$\begin{aligned}
\frac{df_1}{d\eta} &= f_2 \\
\frac{df_2}{d\eta} &= \frac{f_3}{C} \\
\frac{df_3}{d\eta} &= -\frac{f_1 f_3}{C} \\
\frac{ds_1}{d\eta} &= \frac{Pr}{C} s_2 \\
\frac{ds_2}{d\eta} &= -\frac{Pr}{C} f_1 s_2 \\
\frac{dg_1}{d\eta} &= -\frac{Pr}{C} g_2 \\
\frac{dg_2}{d\eta} &= -\frac{Pr}{C} f_1 g_2 - \frac{Ec\,(Pr-1)}{PrC}\left(f_3^2 - f_1 f_2 f_3\right)
\end{aligned} \tag{35}$$

This 1st order system can be solved by generic ODE solvers with one of the following boundary conditions:

- Noncatalytic wall condition
  $\eta = 0$:
  $f_1 = 0,\ f_2 = 0,\ s_2 = 0,\ g_1 = g_w$
  $\eta = \infty$:
  $f_2 = 1,\ g_1 = 1,\ s_1 = 1$

- Fully catalytic wall
  $\eta = 0$:
  $f_1 = 0,\ f_2 = 0,\ s_1 = \left(s_A\right)_{equil},\ g_1 = g_w$
  $\eta = \infty$:
  $f_2 = 1,\ g_1 = 1,\ s_1 = 1$

The results of the DNS code can be compared with this similarity solution by turning off the gas-phase reactions and specifying $C_p = \text{const}$, $Pr = \text{const}$, $Le = 1$, and letting μ be a linear function of T.

For flow over a flat plate with free stream Mach number of 4 with $Le = 1.0$, fully-catalytic isothermal wall with $T_\infty/T_w = 1.0$, $\mu/\mu_\infty = T/T_\infty$ and frozen gas-phase reaction with $N_2 + M \rightleftharpoons 2N + M$, Figure 1 plots non-dimensional velocity and atom mass fraction across the boundary layer. There is good agreement between the numerical results and the similarity solution. The minor discrepancy is due to the presence of leading edge shock effect in the numerical solution while the similarity solution has totally neglected this effect.

5.2 Reacting laminar boundary layer

The constitutive relations and finite-rate gas-phase reaction in the DNS code are validated against DPLR solutions.

For flow over a flat plate with free stream Mach number of 4 with $Le = 1.0$, fully-catalytic isothermal wall with $T_\infty/T_w = 1.0$, $\mu/\mu_\infty = T/T_\infty$ and gas-phase reaction with $N_2 + M \rightleftharpoons 2N + M$, Figure 2 plots non-dimensional velocity and temperature profile assuming vibrational equilibrium and Gupta[9]-Yos[12] mixing rule for mixture transport properties. Agreement is found between the DPLR and DNS code solutions.

5.3 Surface reaction validation

5.3.1 Diffusion tube side-arm reactor

The diffusion tube side-arm reactor [20] in conjunction with laser induced fluorescence for species diagnostics has served as the main method to measure O and N atom recombination coefficients in the range of 300K to 1000K. The diffusion tube consists of a dead-end side-arm tube connected at right angles to a main flow tube, see Figure 3. Free-radical species are produced in the main flow tube upstream of the tube intersection, typically by dissociating molecular gases using some type of low-pressure electrical discharge. The dissociated species flow past the opening of the side-arm tube. As the reactants diffuse into the side-arm tube, they are progressively removed from the gas phase by surface reactions on the wall, establishing a unique steady-state species concentration profile down the length of the tube. This reactor design simplifies subsequent data analysis because gas transport in the side-arm is restricted to species diffusion.

A surface chemistry model is needed to fit experimental data by adjusting the model parameters to reproduce experimental results. In the case of binary atom-molecule system, assuming a purely catalytic wall and a single heterogeneous loss pathway leading to atom recombination, one simple reaction-diffusion model that can be applied to evalute surface recombination is obtained by solving the linear one dimensional diffusion equation with surface loss included as a first-order sink term:

$$D\frac{\partial^2 n}{\partial x^2} - \dot{R}_{sink} = 0 \tag{36}$$

where $\dot{R}_{sink} \equiv$ (loss probability)(atom surface impingement rate)(surface area per volume), or

$$\dot{R}_{sink} = \gamma\left(\frac{\bar{v}n}{4}\right)\left(\frac{2\pi R dx}{\pi R^2 dx}\right) = \left(\frac{\gamma\bar{v}}{2R}\right)n \tag{37}$$

Here n is the atom number density, x is the axial tube coordinate, R is the tube radius. In the case of constant atom concentration at the tube entrance and infinite long tube, a simple simple solution can be obtained:

$$\frac{n(x)}{n(0)} = exp\left(-x\sqrt{\frac{\bar{v}\gamma}{2DR}}\right) \tag{38}$$

5.3.2 Numerical results

The numerical solution is obtained by solving two-dimensional cylindrical diffusion-reaction equation of species s:

$$\frac{1}{r}\frac{\partial}{\partial r}\Big(r j_{sr}\Big) + \frac{\partial}{\partial x}\Big(j_{sx}\Big) = 0, \tag{39}$$

where j_{sr} and j_{sx} are the diffusive mass fluxes in the radial and axial directions, which are computed by SCEBD, described in Section 2.1.2, and the surface boundary conditions are described in Section 3. The computation domain is chosen to be the same as the side-arm reactor geometry in Stanford Research Institute (SRI) International, with tube length $L = 146.7$cm and uniform radius $R = 1.1$cm, closed at one end by a disk normal to the tube axis.

Figure 4 gives the comparison of numerical results with analytic results described in 5.3.1 for $\gamma = 10^{-5}$, $T = 298$K, $P = 0.45$Torr, and $\bar{v} = 671.12\text{m}^2/\text{s}$. The analytic solution is obtained for an infinitely long tube. However, the tube in the simulations is of finite length. Thus, small discrepancies are observed due to the end-tube effects for the simulation.

5.4 Turbulent boundary layer

The code has been validated for turbulent boundary layers including chemical reactions [21, 4]. Figure 5 plots the van Driest transformed velocity profiles in turbulent boundary layers for DNS varying free stream Mach number and wall-temperature condition [21, 22]. The symbols show the theoretical values, illustrating the good accuracy of the simulations. An index of the flow accuracy at the wall is given by the skin friction coefficient, C_f. Figure 6 plots C_f for the same simulations relative to the empirical predictions [23]. The error bars show a 7% error where the error in the empirical prediction is 10%. Figure 6 further illustrates the accuracy of the simulations, specifically at the wall. This degree of accuracy is necessary to study the interaction between the boundary layer flow and gas phase and the surface chemistry.

6 Conclusion

This paper describes the constitutive relations and surface catalytic model in a DNS code for wall-bounded turbulence including finite-rate gas-phase and surface reactions. Both the mean flow and turbulence field are validated, indicating that the code can be used for analyzing chemically reacting turbulent flow including wall catalysis.

Acknowledgments

This work is sponsored by the Air Force Office of Scientific Research, USAF, under Grant FA9550-05-1-0490. Computational resources are provided by the CRoCCo Laboratory at Princeton University.

References

[1] M.P. Martin and G.V. Candler. DNS of Mach 4 boundary layer with chemical reactions. *AIAA Paper No.2000-0399*, 2000.

[2] M.P.Martin and G.V. Candler. Temperature fluctuation scaling in reacting turbulent boundary layers. *AIAA Paper No.01-2717*, 2001.

[3] M.P Martin. Exploratory studies of turbulence/chemistry interaction in hypersonic flows. *AIAA Paper No.03-4055*, 2003.

[4] M.P. Martin and G.V. Candler. Effect of chemical reactions on decaying isotropic turbulence. *Physics of Fluids*, 10(7):1715–1724, 1998.

[5] M.P. Martin and G.V. Candler. Subgrid scale model for the temperature fluctuations in reacting hypersonic turbulent flows. *Physics of Fluids*, 11(9):2765–2771, 1999.

[6] M.J. Wright, G.V. Candler, and D. Bose. Data-parallel line relaxation method for the navier-stokes equations. *AIAA*, Vol.36:1603–1609, 1998.

[7] D.A. Pejakovic, J. Marschall, L. Duan, and M.P Martin. Nitric oxide production from surface recombination of oxygen and nitrogen atoms. *Accepted for publication in Journal of Thermophysics and Heat Transfer*, 2008.

[8] J.D. Ramshaw. Self-consistent effective binary diffusion in multicomponent gas mixtures. *Journal of Nonequilibrium Thermodynamics*, 15(3):295–300, 1990.

[9] R.N. Gupta, J.M. Yos, R.A. Thompson, and K.-P. Lee. A review of reaction rates and thermodynamic transport properties for an 11-species air model for chemical and thermal nonequilibrium calculations to 30,000 k. *NASA RP-1232*, 1990.

[10] M.J. Wright, E. Levin, and D. Bose. Recommended collision integrals for transport property computations iii: Giant planet entries. *AIAA Journal in Preparation*, 2005.

[11] J.O. Hirschfelder. Heat conductivity in polyatomic or electronically excited gases ii. *Journal of Chemical Physics*, 26(2):282–285, 1957.

[12] J.M. Yos. Transport properties of nitrogen, hydrogen, oxygen, and air to 30,000 k. *Avco. Corp. TR AD-TM-63-7*, 1963.

[13] C. Park. Nonequilibrium hypersonic aerodynamics. *Wiley*, 1990.

[14] V.G. Weirs and G.V. Candler. Optimization of weighted eno schemes for dns of compressible turbulence. *AIAA Paper No.1997-1940*, 1997.

[15] E.M. Taylor, M. Wu, and M.P Martin. Optimization of nonlinear error sources for weighted non-oscillatory methods in direct numerical simulations of compressible turbulence. *Journal of Computational Physics*, 223:384–397, 2006.

[16] M.P. Martin, E.M. Taylor, M Wu, and V.G. Weirs. A bandwidth-optimized WENO scheme for the effective direct numerical simulation of compressible turbulence. *Journal of Computational Physics*, 220:270–289, 2006.

[17] M.P. Martin and G.V. Candler. A parallel implicit method for the direct numerical simulation of compressible flows. *Journal of Computational Physics*, 215(1):153–171, 2006.

[18] J.A Fay and F.R. Riddell. Theory of stagnation point heat transfer in dissociated air. *Journal of Aeronautical Sciences*, 25(2):73–85, 1958.

[19] J.D Anderson. Hypersonic and high temperature gas dynamics. *McGraw-Hill*, 1989.

[20] W.V. Smith. The surface recombination of H atoms and OH radicals. *Journal of Chemical Physics*, 11:110–125, 1943.

[21] M.P. Martin. DNS of hypersonic turbulent boundary layers. part i: Initialization and comparison with experiments. *Journal of Fluid Mechanics*, 570:347–364, 2007.

[22] M.P. Martin. DNS of hypersonic turbulent boundary layers. *34th AIAA Fluid Dynamics Conference*, 2004.

[23] E. Van-Driest. Problem of aerodynamic heating. *Aeronautical Engineering Review*, 15:26–41, 1956.

Reaction	C_{fm} (m^3/kg s)	η_m	θ_{dm} (K)
R_1	1.11d+16	-1.60d+00	113200
R_2	8.25d+13	-1.00d+00	59500
R_3	2.30d+11	-0.50d+00	75500
R_4	3.18d+07	-0.10d+00	37700
R_5	2.16d+02	+1.29d+00	19220

Table 1: Arrhenius parameters for the two-species, one reaction mechanism[13] and five-species, five-reaction mechanism[13]. The corresponding equilibrium constants are computed from the Gibbs free energy as functions of temperature and then fitted to Park (1990) expressions.[13]

Case	A_1	A_2	A_3	A_4	A_5
R1	1.60600d+00	-1.57320d+00	1.39230d+00	-1.15530d+01	-4.54300d-3
R2	6.41830d-01	2.42530d+00	1.90260d+00	-6.6277d+00	3.51510d-02
R3	6.38170d-01	6.81890d-01	6.63360d-01	-7.57730d+00	-1.10250d-02
R4	9.67940d-01	8.91310d-01	7.29100d-01	-3.95550d+00	6.48800d-03
R5	-3.73200d-03	-1.74340d+00	-1.23940d+00	-9.49520d-01	-1.46341d-01

Table 2: Equilibrium constants computed from the Gibbs free energy as functions of temperature and then fitted to Park (1990) expressions.[13]

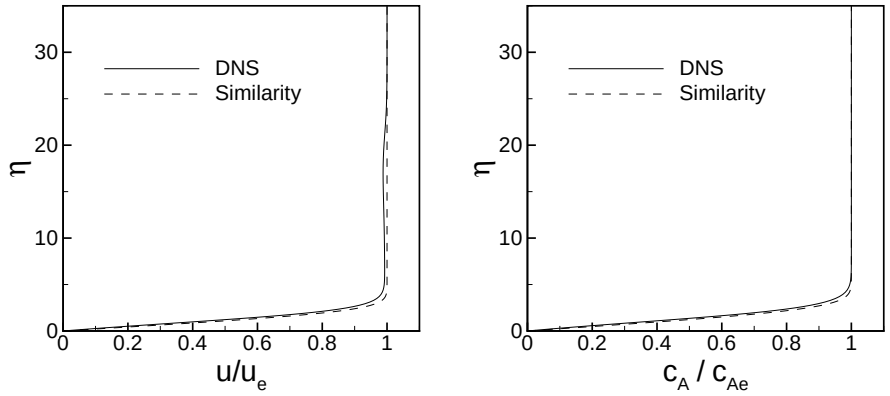

Figure 1: comparison of numerical and similarity solution with $Ma_\infty = 4$, $Le = 1$, fully-catalytic isothermal wall with $T_\infty/T_w = 1$, $\mu \propto T$,no gas-phase reactions. Left: Velocity profile; Right: Atom mass fraction profile

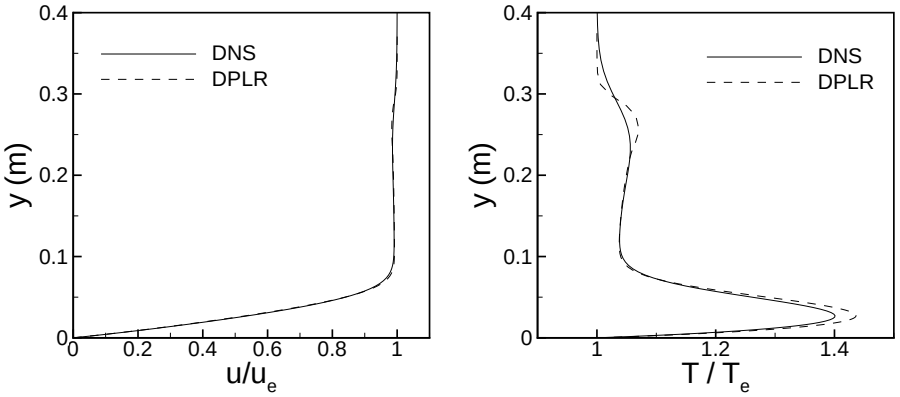

Figure 2: comparison of numerical and similarity solution with $Ma_\infty = 4$, $Le = 1$, non-catalytic isothermal wall with $T_\infty/T_w = 1$, $Re_\infty = 5101$. Left: Velocity profile; Right: temperature profile

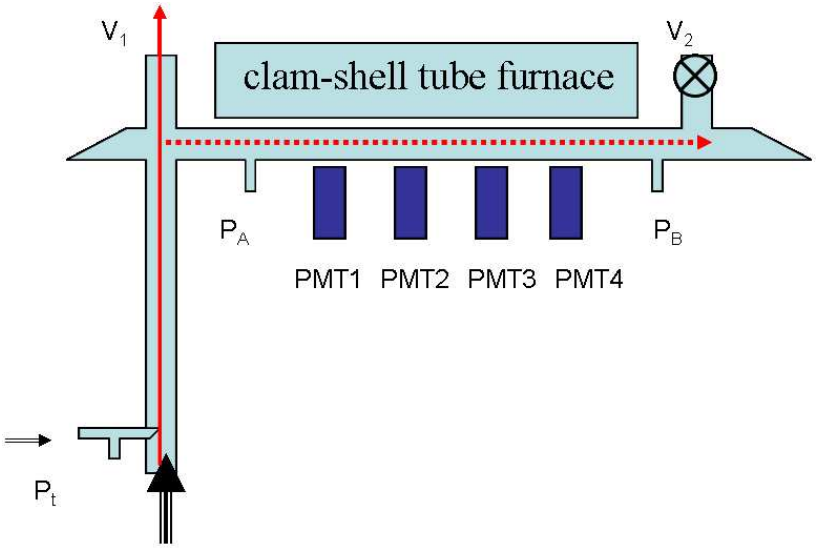

Figure 3: Schematic diagram of a diffuse-tube side-arm reactor

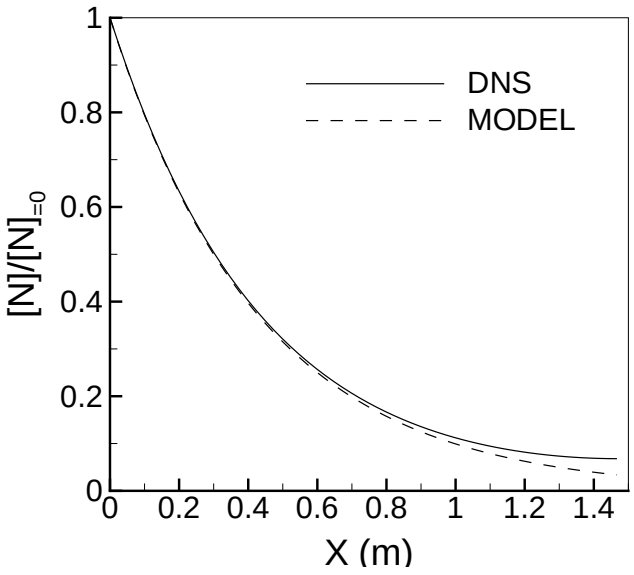

Figure 4: Scaled nitrogen atom concentration along the diffusion tube with recombination coefficient $\gamma = 10^{-5}$, temperature $T = 298$K, pressure $P = 0.45$ Torr, $\bar{v} = 671.12\text{m}^2/\text{s}$

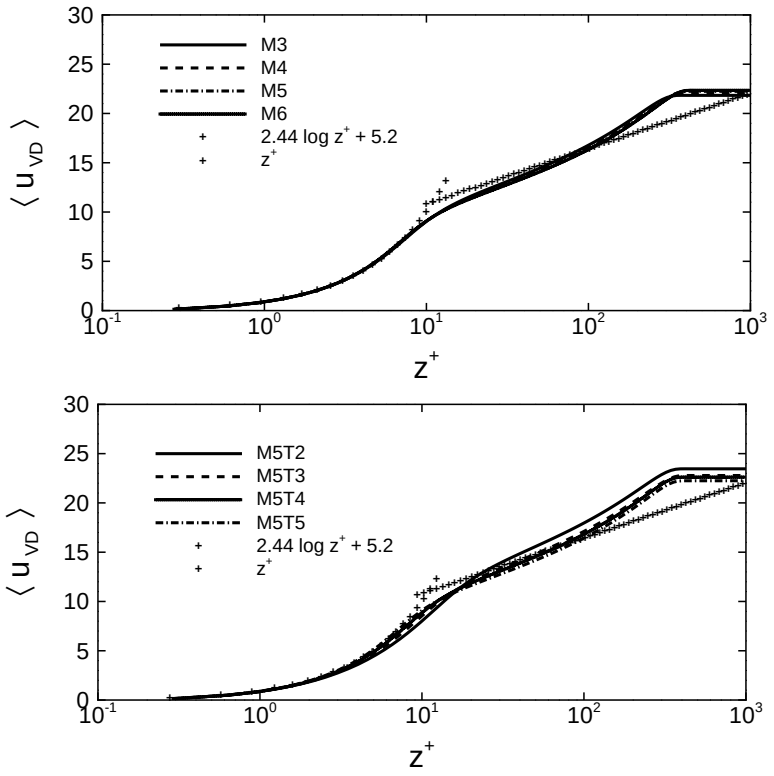

Figure 5: Van Driest Transformed velocity in turbulent boundary layers varying (a) free stream Mach number from [21, 22] and (b) wall-temperature from DNS from [22]

.

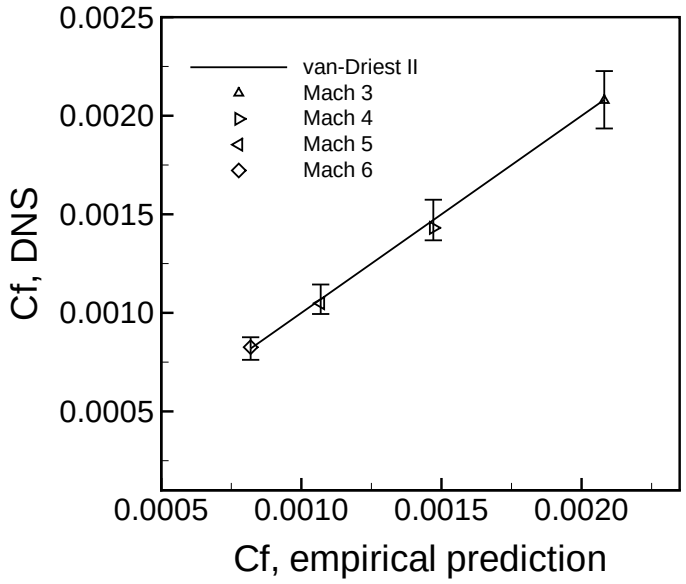

Figure 6: Skin friction coefficient for hypersonic turbulent boundary layer for DNS.